JFBE 5(1): 16-23, 2022

Journal of Food and Bioprocess Engineering

Journal homepage: https://jfabe.ut.ac.ir

Original research

Experimental study of the passage of canola oil and olive oil droplets between the water-oil interfaces

Safoora Karimi*, Ana Abiri, Mojtaba Shafiee

Department of Chemical Engineering, Jundi-Shapur University of Technology, Dezful, Iran

ABSTRACT

Today, the discussion of droplet-fluid interaction is one of the most challenging topics in multiphase (liquid-liquid) flows. In the present study, the behavior of two edible oils (olive oil and canola oil) droplets during the rising in the static fluid of water and passing through the water-oil interface was experimentally investigated. Droplet diameters were controlled in the range of 3.8 to 5.6 mm. First of all, the range of dimensionless numbers was compared to experimental data from other researchers and validated. The results revealed that the droplet shape is elliptical, and that the Weber number decreases in the range of 1 to 2, as the aspect ratio increases. Furthermore, the droplet residence time at the two-phase interface was measured, and the parameters that affected it were examined. Although the results showed that the residence time did not follow a consistent pattern, the conclusion was not far off. Weber dimensionless number was used to introduce hydrodynamic forces and internal surface tension of the droplets. It was shown that none of the theoretical relationships can accurately or even roughly predict the residence time of the oil droplets. Finally, the Weber number has been proven to be dependent on the droplet terminal velocity. Terminal velocity increases with the Weber number and the equivalent diameter.

Keywords: Liquid-liquid interface; Residence time; Droplet aspect ratio; Weber number

Received 3 February 2022; Revised 18 April 2022; Accepted 19 April 2022

1. Introduction

Vegetable oils are a type of fat found in seeds, nuts, oil-rich fruits, and cereals. These are one of the most widely used ingredients in food industry. Todays, spread of these oil droplets in industrial and domestic wastewater is one of the environmental issues. Therefore, understanding the behavior of the droplets in the presence of a second fluid (for example at their interface) will be beneficial in developing effective purification methods. Moreover, it would be crucial in processes such as liquid-liquid extraction, flotation, filtration, detergent production and emulsification. Oil droplets suspended in liquid eventually move to the interface between two phases and form a layer on the water's surface due to their lightness. Determining the required time for the formation of this layer as well as its thickness is of great importance in interface studies (Mottola et al., 2019). One of health degradation identified by Brakstad et al. (2015) is the appearance of oil droplets in deep water during the oil extraction process. They stated that in deep water, the surface tension between gas, oil, and liquid causes to form droplets with different sizes. In general, the knowledge of oil droplet behavior is applicable to a wide range of phenomena including health science, environmental science, and technology. The oils that are the subject of this study are olive and canola oils. These are monounsaturated fats which not appear to enhance the risk of cancer in the same way as polyunsaturated fats, corn oil, and meat do.

Canola oil primarily is used in a variety of food preparations, including baking, frying, salad dressings, and confectionery making. It is obtained from a type of rapeseed. In some countries, such as Canada, canola oil has been substituted for other oils due to its health-friendly properties (Marcus, 2013; Asokapandian et al., 2021). Olive oil is another widely used edible oil. In Mediterranean diets, it is very important due to its anti-cancer properties (Gorzynik-Debicka et al., 2018). The diet is very interesting for the prevention and treatment of diseases such as colorectal cancer (Borzì et al., 2019), breast cancer (Stark & Madar, 2021) and skin cancer (Psaltopoulou et al., 2011). Extra-virgin olive oil is used for appetizers, dips, salads, and vegetables. Virgin olive oil is used for all-purpose cooking, margarine and salad dressing. Refined and

*Corresponding author.
E-mail address: s.karimi@jsu.ac.ir (S. Karimi).
https://doi.org/10.22059/jfabe.2022.338502.1109

extra-light olive oil can use for sautéing and stir-frying because of its high heat withstand ability in compare to extra-virgin olive oil. All of the above-mentioned advantages of these two oils were the driving force behind their selection for this study.

According to our knowledge, studies on droplet motion at the interface of two fluids are still scarce. Sternling and Scriven (1959) made the first theoretical attempt to predict interfacial instability in a liquid-liquid system. Other researchers later conducted more comprehensive theoretical studies (Hennenberg et al., 1979; Hennenberg et al., 1980; Nakache et al., 1983; Slavtchev et al., 1998; Slavtchev et al., 2006; Slavtchev & Mendes, 2004; Blanchette & Bigioni, 2009). For instance, Deng et al. (2020) investigated the attachment of a droplet to a liquid-liquid interface. They stated that droplet coagulation was delayed as the interface moved faster. Recently, Karimi et al. (2020) investigated the passage of crude oil droplets through the water-oil interface. They demonstrated that the drop shape is ellipsoidal in the applied conditions, and that the value of Weber's number decreases as the aspect ratio of the drop increases. In general, when droplets approach the interface of two phases, they may appear to "float" for a few seconds, as first reported by Reynolds (1881). The phenomenon piqued the interest of some researchers, who attempted to measure or calculate the residence time of droplets at the interface of two phases (Charles & Mason, 1960; Cockbain & McRoberts, 1953; Gopinath & Koch, 2002; Linton & Sutherland, 1956). A silicone-water mixture was also used as a drop by Mohamed-Kassim and Longmire (2003). Generally, studies show that when a droplet must be adsorbed and disappear to the bulk's surface, various factors such as size, shape, and droplet velocity all have an impact on how it behaves. Moreover, droplet deformation affects not only the interface between the two phases and thus the mass transfer rate, but also the drag coefficient and consequently the terminal velocity (Grace, 1976).

As can be seen, while many studies have been done on the motion of a single droplet in a bulk liquid, a complete study of its residence time, particularly for edible oil droplets at the interface of two fluids, has yet to be done. Therefore, experimental observations of the oil droplet transport phenomenon from the water-oil interface are presented in this study. Here, the residence time parameter of two widely used edible oil droplets (canola and olive oil) at the water-oil interface was examined and evaluated. For example this information, will be extremely useful in systems such as oil refinery wastewater treatment and industrial food production. The presence of excess oil droplets in these systems and the need to remove them to prevent them from entering the environment is one of the cases that show the importance of studying and comparing oils in these systems. In general, this information, along with all the physicochemical and nutritional properties of these oils, can help to select them in the industry. The parameters which are calculated were diameter, shape, and residence time. Rising velocity of droplets as well as some dimensionless groups, such as Reynolds, Eötvös and Morton numbers were also analyzed.

Table 1. Physical propertied of materials used in experiments.

Physical parameters	water	olive oil	canola oil
ρ (kg/m^3)	1000	842	854
μ (cp)	0.98	0.039	0.034
σ (N/m)		0.0243	0.0275

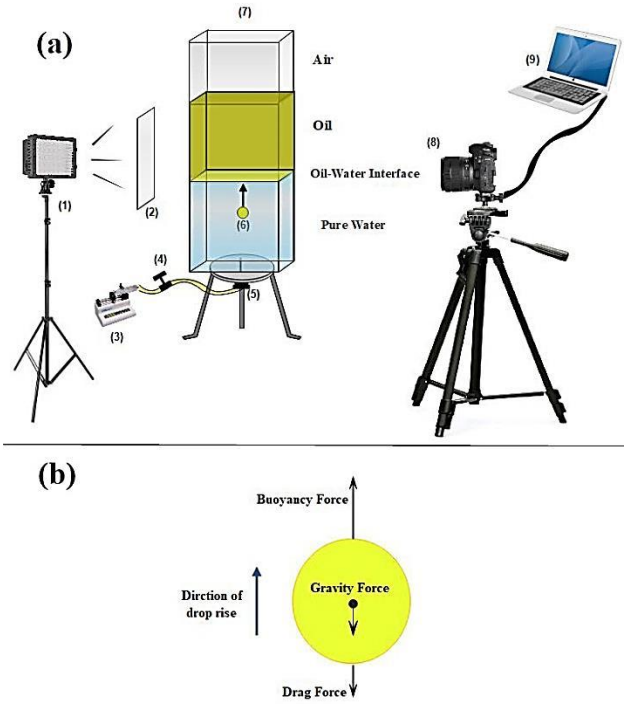

Fig. 1. (a) Schematic of experimental apparatus, 1: LED lamp, 2: Diffuser, 3: One -way valve, 4: Syringe pump, 5: Needle, 6: Bubble rising in the liquid column, 7: liquid column, 8: Camera and macro lens, 9: Image processing system, (b) applied forces on the surface of the rising droplet.

2. Material and Methods

2.1. Experimental set-up

All experiments were done at ambient temperature and atmospheric pressure. The laboratory set for this project is depicted schematically in Fig.1(a). A vertical column made of Plexiglas with a height of 500 mm and an internal cross section of 80×80 mm^2 is included in the set-up. Half of the column is filled with distilled water and the other half with other oils, such as olive or canola oils, to a height of 400 mm. The test area is the meeting point of two phases, where an oil droplet passes through the bulk water and into the oil phase. The column is large enough so that the effects of its walls on the droplet motion can be neglected. The top of the column is exposed to the free atmosphere. The needle, whose internal diameter ranged from 0.6 to 1.6 mm, controls the oil droplet diameter. The needle is connected to a syringe pump, which is used for oil injection, by a flexible tube. Oil droplets were injected into the column at a rate of 0.4 ml/min, which is low enough to prevent two consecutive droplets from interacting. As previously stated, the fluids used are distilled water at room temperature and olive and canola oils, whose physical properties are listed in Table 1.

The canola oil and olive are made with different fatty acids. The range of weight percent of monounsaturated, polyunsaturated and saturated fatty acids in canola oil and olive oil are listed in Table 2.

Table 2. Chemical composition of different fatty acids in canola oil and olive oil.

Weight percentage	Canola oil	Olive oil
Saturated fatty acids	0.8-3	0.5-5
Monounsaturated fatty acids	51-70	55-83
Polyunsaturated fatty acids	15-30	3.5-21

High-resolution photographs of the droplets were captured using a camera with a 100 mm macro lens (AT-X M100 Pro, Tokina, Japan). The camera was placed vertically in front of the column, exactly opposite the interface of the two phases, as illustrated in Fig. 1(a). A semi-transparent diffuser was placed between the column and a LED lamp to increase picture processing quality and reduce light reflection by rising droplets. The diffuser not only evenly distributes light across the liquid column, but also prevents the test region from heating. The precise location of the diffuser was determined manually through a series of tests. Each experiment was repeated at least three times in order to reduce experiment error, and their average results were used as the final result.

2.2. *Image Processing*

First, Video image master V1.2.5 software was used to convert the captured video into a series of images at various times. Then, geometric parameters, location of the droplet and duration of its disappearance in the oil phase were calculated by analyzing the obtained image collection. After that, with the help of Image J V1.51 software, the images were cut in the desired range and the boundary between the droplet and fluid is determined. Finally, velocity, center position, and aspect ratio of the droplet as well as its disappearance time in the oil bulk were obtained. The authors have already verified the results obtained using this method (Karimi et al., 2019).

2.3. *Calculating dimensionless numbers*

In the present work, parameters such as dimensionless numbers such as Weber $We = \rho_l V_t^2 d_{eq}/\sigma$, Reynolds $Re = \rho_l d_{eq} V_t/\mu_l$, Eötvös $Eo = (\rho_l - \rho_d) g d_{eq}^2/\sigma$ and Morton $Mo = g\mu_l^4(\rho_l - \rho_d)/\rho_l^2\sigma^3$, equivalent diameter, aspect ratio and retention time were calculated, which are evaluated in the following.

The equivalent diameter is the diameter of a sphere whose surface area is the same as the surface area of the droplet, thus $d_{eq} = \sqrt{4A/\pi}$ where A is the droplet's represented surface. The aspect ratio (E) is defined as the ratio of the biggest vertical diameter (90^o angle with the horizontal axis) to the maximum horizontal diameter (0^o angle with the horizontal axis) of a droplet. The residence time of the droplet on the interface between the two fluids continues until it disappears in the oil bulk phase.

One of the effective characteristics in the flow pattern is Weber number, which reveals the effects of surface tension. In general, when the Weber number rises, the deformation of the droplet during flow increases, and the droplet's internal rotation is abolished. It is used to calculate the diameter of a drop, its interfacial surface, and breakup.

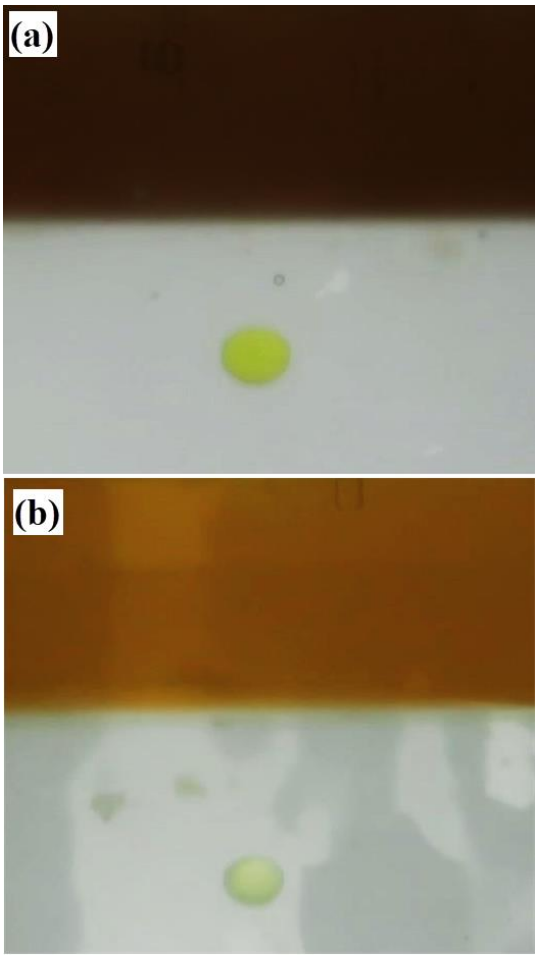

Fig. 2. Image of different oil droplets rising in water before attach to the water-oil interface (a) canola oil droplet, (b) olive oil droplet.

3. Results and Discussion

In order to study the rising behavior of a floating droplet and its attachment to the interface of the two phases, applied forces on it should be investigated. The main forces acting on the rising droplet's surface are shown in Fig.1(b). These forces are gravity, drag, and buoyancy. The buoyancy force, rather than the surface tension force that causes the droplet to connect to the nozzle, is the main driver of the droplet separating from the nozzle and rising. As soon as the droplet is fully produced with the desired size and separated from needle, it rises due to the resultant forces.

In such circumstances, not only the interfacial tension but also the diameter of the nozzle controls the droplet volume. Here due to the presence of oil on the top of water, the pressure at the bottom of the column increases and as a result, the rising of the oil droplet is delayed. Moreover, the surface tension force in liquids causes their outer layer act as an elastic layer (Mao et al., 2020). It causes the two liquid surfaces to adsorb each other, as a result in the oil droplets are attached to the interface (Clift et al., 1978).

Table 3. Dimensional numbers of Reynolds, Eötvös and Morton in different nozzle for droplets canola and olive oil.

	Diameter of Needle (mm)	d_{eq} (mm)	Re	Eo	Mo
Olive oil	0.6	3.88	325.35	0.96	9.95E-11
	0.8	4.29	372.52	1.17	9.95E-11
	1.2	5.14	468.03	1.68	9.95E-11
	1.6	5.35	496.92	1.83	9.95E-11
Canola oil	0.6	4.23	364.39	0.93	6.35E-11
	0.8	4.63	415.70	1.12	6.35E-11
	1.2	5.18	483.48	1.40	6.35E-11
	1.6	5.52	522.35	1.58	6.35E-11

Table 4. The aspect ratio and equivalent diameter of oil droplets in different diameters of needle.

Needle Size (mm)	d_{eq} (mm)		E	
	Olive oil	Canola oil	Olive oil	Canola oil
0.6	3.89	4.23	0.924	0.953
0.8	4.29	4.63	0.915	0.918
1.2	5.14	5.18	0.893	0.881
1.6	5.35	5.52	0.885	0.876

Table 5. The Weber dimensionless number of canola oil and olive oil in different nozzle diameters.

Needle diameter (mm)	Canola oil		Olive oil	
	We	d_{eq} (mm)	We	d_{eq} (mm)
0.6	1.096	4.23	1.079	3.89
0.8	1.304	4.63	1.280	4.29
1.2	1.575	5.18	1.684	5.14
1.6	1.727	5.52	1.823	5.35

In this study, the shape characteristics and residence time of the droplet at the two phase interface have been investigated. The dimensionless numbers that were considered in order to reflect these forces are Reynolds, Eötvös, and Morton, which are the most common numbers in the study of single bubble or droplet behavior (Karimi et al., 2020; Zhang et al., 2018). In the present study, the dimensionless numbers are given in Table 3.

To begin, the range of dimensionless numbers was compared to Grace's experimental data (Grace, 1973) to confirm the findings of the present study. His experimental results which cover a wide range of Reynolds, Eötvös and Morton numbers provide a relationship between the three dimensionless numbers. Accordingly, for the Reynolds and Eötvös range of the present work ($350 < Re < 550,\ 0.85 < Eo < 1.83$), the Morton number should be in the range of 6.3×10^{-11} to 1×10^{-10}, which is consistent with the results presented in Table 3.

3.1. Aspect Ratio of droplet

Fig. 2 depicts the actual image of a rising droplet in water near the water-oil interface for two oils when the needle diameter is 1.6 mm. In both cases, the oil droplet is almost ellipsoidal, as shown in the figure. Its calculated values for all experiments are summarized in Table 4.

The aspect ratio of spherical particles is one by definition; as the number decreases, the droplets lose their spherical shape and become elliptical. The droplet will be in the form of tear when the ratio approaches zero. Table 4 shows that in the present experiments the oil droplets are almost ellipsoidal, and droplet's aspect ratio falls as the nozzle diameter increases. In other words, as the oil droplet grows larger, its shape becomes less spherical. The conclusion on the droplet rising into the pure water is relatively consistent with the results of Rao et al. (2014). According to Rao et al. (2014), aspect ratio for a droplet motion in liquid water is 0.85, which is nearly identical to the results of the present work. The only observed discrepancies are due to the materials used, the presence of surfactant in their work, and the nozzle size in the two works. Furthermore, Rao et al. (2014) demonstrated that the shape of an oil droplet in pure water is almost elliptical and its size decreases when a surfactant is added. The variation of aspect ratio versus droplet equivalent diameter is seen in Fig. 3. As shown in Fig. 3, the aspect ratio decreases almost linearly with the equivalent diameter. According to the study of Rao et al. (2014), Due to the absence of surfactant in the continuous phase, the shear force is increased and the shape of the droplets to overcome the effects of hydrodynamic forces is not completely spherical. Mohamed-Kassim and Longmire (2003) findings also reveal that near the surface, at high Reynolds numbers, droplet takes on a wider and ellipsoidal shape. This result is consistent with the current experiments' observations and data. Wang et al. (2018) also investigated the motion of a coated bubble with octane and silicon oil through a fluid, and found that for bubbles with diameters

between 3.9 and 5.5 mm, the aspect ratio drops from 0.95 to 0.87 as the diameter increases, which is consistent with the results shown in the current figure.

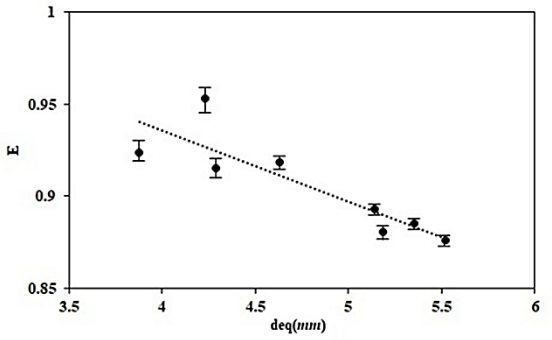

Fig. 3. Dependence of the droplet aspect ratio to the equivalent diameter, near the interface.

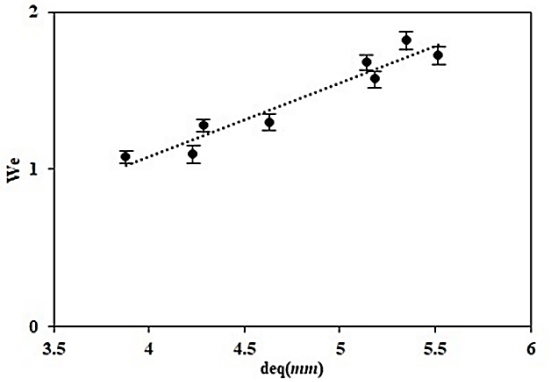

Fig. 4. Weber number variations versus droplet equivalent diameter.

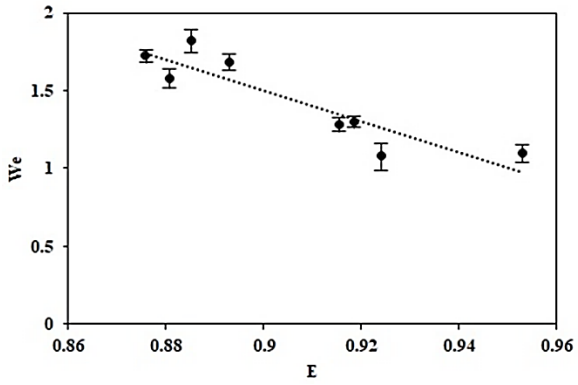

Fig. 5. Dependence of Weber number on aspect ratio.

In the present work, water is employed as a continuous phase, whereas oil droplets are used as a dispersed phase. Therefore, the oil droplet rises due to the density difference between the continuous and dispersed phases, and when it reaches the phase interface, the kinetic energy of its motion causes the oil droplets to bind to the oil bulk (Zawala et al., 2007). Different shapes of droplet are created by applying kinetic energy to the surface of the droplet. Generally, the droplet is usually drawn to the interface, and then it may split into smaller secondary droplets. Some conditions such as residence time and droplet size must be considered before attaching the droplet to the interface (Komrakova, 2019). The interaction of hydrodynamic forces due to turbulence and surface tension between the droplet and the surrounding fluid plays a vital role in the research of droplet attachment. Weber dimensionless number expresses the relationship between the hydrodynamic force and the droplet's internal surface tension.

As results, the larger oil droplet, the higher Weber number, indicate that the hydrodynamic force dominates the internal surface tension of the droplet reduce the droplet's residence time in the interface. The Weber dimensionless number for various droplets size is shown in Fig. 4 and Table 5.

According to Fig. 4, Weber number depends on the equivalent diameter of the droplet. The greater nozzle diameter and consequently the larger oil droplet, the higher Weber number, indicating that the hydrodynamic force is greater than the internal surface tension force of the droplet, reducing the residence time on the interface two phase. In addition, a comparison of the results derived from Fig. 3 and 4 illustrates that as the aspect ratio increases, the Weber number decreases, as shown in Fig. 5.

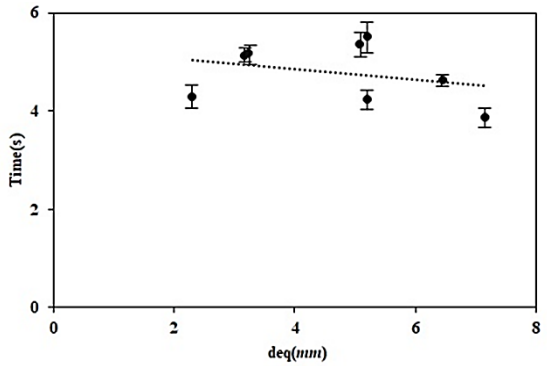

Fig. 6. Variation of residence time versus droplet diameter.

3.2. *Residence time of droplet on the interface*

Fig. 6 shows the obtained residence time of the droplet on the two-phase interface. As can be observed, the relationship between them does not follow a consistent pattern. Actually, as the droplet diameter enhances, the droplet velocity increases to reach the two-phase interface. This accelerates the formation of a common layer between the two phases, resulting in a shorter residence time. On the other hand, as the droplet's volume grows, the liquid volume available to connect to the above liquid enhances, therefore it takes more time to disappear. Non-uniformity in residence time has resulted from these two opposing impacts. Furthermore, the contact of the droplet with the two-phase boundary causes it to become unstable and wavy. In this case, the interface stores and subsequently releases the energy of the collision (Singh et al., 2017). The wave is also highly effective in non-uniformity of residence time. A similar result has been observed by Singh and Bart (2020), where the disappearance of bubbles at the interface of fluids with a density difference approximately similar to the present work was studied. Moa et al. (2020) also found similar non-

uniformity in their study of bubble motion at the water-oil interface. Besides, Karimi et al. (2020) demonstrated that in the study of oil droplet passage through the water-oil interface, the droplet's residence time does not follow a predictable pattern.

Because of the non-uniformity of the residence time, as was discussed in the preceding section, only a few experimental equations have been provided to calculate the time at the two-phase interface for droplets. Some of these equations are discussed in this section. The Stephen-Reynolds relationship (Sinegribova et al., 1993) is the first to be presented:

$$t = \frac{\mu_l \Delta\rho g d_{eq}^2}{4\sigma^2 L^2} \quad (1)$$

where *L*, the distance of falling (or rising) of droplet and the liquid-liquid interface, is assumed to be rigid, and the wave caused by the collision of droplet is ignored. Hartland (1988) also presents a theoretical-empirical relationship for calculating residence time as follows:

$$t = \frac{3}{16\pi} n^2 \mu_l \left(\frac{d_{eq}^2}{\sigma}\right)\left(\frac{1}{L^2}\right) \quad (2)$$

where *n* is the number of static surfaces that interfere with the development of the generated layer during droplet attachment. Jeffreys and Davies (1971) and Smith (Laddha & Degaleesan, 1983) developed similar relationships to compute the residence time with independent variables.

$$t = 1.32 \times 10^5 \left(\frac{\Delta\rho g d_{eq}^2}{\sigma}\right)^{0.32} \left(\frac{L}{d_{eq}}\right)^{0.18} \left(\frac{\mu_l d_{eq}}{\sigma}\right) \quad (3)$$

$$t = 3.1 \times 10^3 \left(\frac{\Delta\rho g d_{eq}^2}{\sigma}\right)^{-1.24} \left(\frac{\mu_d}{\mu_l}\right)^{1.03} \left(\frac{\mu_l d_{eq}}{\sigma}\right) \quad (4)$$

Khadiv (2004) also provides a relation as follows:

$$t = 4.846 \times 10^3 \left(\frac{\Delta\rho g d_{eq}^2}{\sigma}\right)^{1.512} \left(\frac{L}{d_{eq}}\right)^{0.651} \left(\frac{\mu_d}{\mu_l}\right)^{0.203} \left(\frac{\mu_l d_{eq}}{\sigma}\right) \quad (5)$$

Among these equations, only the Smith equation (Eq. 4) predicts a decrease in residence time as a function of droplet diameter. Furthermore, a comparison of the current experimental data with the previous equations reveals that, none of them accurately captures the current experiments' residence time trend.

3.3. *Terminal Velocity*

The terminal velocity is the rate at which the rising drop velocity remains constant (approximately at a height of 175 mm above the column). Karimi et al. (2020) have already given a detailed explanation of how it is calculation procedure. The drop terminal velocity is shown in Fig. 7 as a function of its equivalent diameter. Accordingly the terminal velocity tends to increase as the equivalent diameter increases. For bubble equivalent diameters of 3.8–5.6 mm, the terminal velocity is in the range of 82-94 mm/s. A similar trend was documented by Deng et al. (2018). The more comparable diameter led to the higher the terminal velocity, according to Zheng *et al.* (2020). Their comparable bubble diameter ranges from 1.5 to 5 mm, and their terminal velocity ranges from 160 to 230 mm/s. In their study, due to the presence of surfactant, a "Marangoni effect" has been created. Therefore, the terminal velocity has increased compared to the present work. Also, Kurimoto et al. (2013) showed that terminal velocity $80 < V_t < 580$ mm/s increases with increasing equivalent diameter $2 < d_{eq} < 9$ mm. Azizi et al. (2017) examined the presence of a drop in a fluid (Deionized water with Toluene-acetic acid), they showed, for $4 < d_{eq} < 6.5$ mm the terminal varies between 70 and 82 mm/s, they showed, that the range of present work is close to this data.

Fig. 8 depicts terminal velocity as a function of weber number. The Weber number rises with increasing terminal velocity. This finding was not surprising, given the direct link between terminal velocity and equivalent diameter in the Weber number equation.

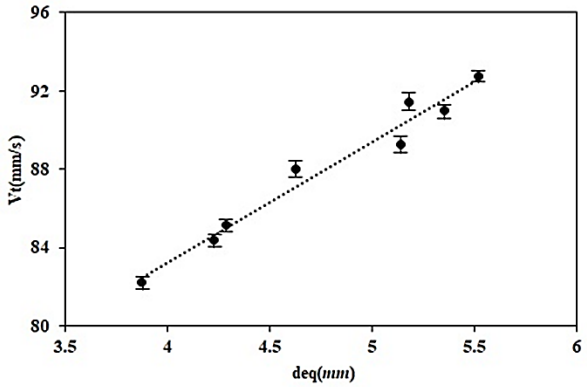

Fig. 7. Dependence of the terminal velocity on the equivalent diameter.

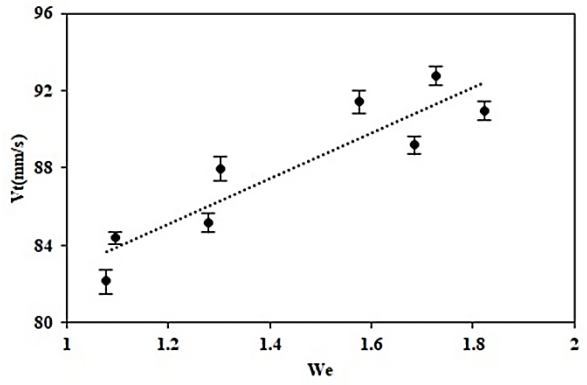

Fig. 8. Drop terminal velocity versus Weber number.

4. Conclusion

In the present study, the motion of two types of canola and olive oil droplets in a static fluid of water and its passage through the water-oil interface was investigated. The motion of the droplets in was recorded by a camera, which was then processed to generate the data, which included aspect ratio, residence time, and dimensionless numbers like Weber number. The results demonstrate that the shape of the rising oil droplet is elliptical, which is owing to the applied forces to the oil surface. Furthermore, the findings showed that by increasing the size of the oil droplet, its

shape becomes farther from the spherical state. Hydrodynamic forces and internal surface tension of the droplet are introduced using Weber dimensionless number. Accordingly, it can be concluded that as the droplet diameter increases, Weber number increases, and as a result, the hydrodynamic force dominates the droplet's internal surface tension force, reducing the droplet's retention time at the water-oil interface. The droplet residence time does not follow a uniform trend due to the contrast between a reduction in residence time resulting in an increase in velocity for larger droplet diameter and an increase in disappearance time due to an increase in droplet volume. An analysis is performed on the proposed theoretical equations. Accordingly, it is not possible to use the previous equations due to the residence time is strongly influenced by the viscosity of the continuous phase. Finally, it has been shown that the Weber number depends on the droplet terminal velocity. Terminal velocity increases with the Weber number and the equivalent diameter.

Acknowledgment

Not applicable.

Conflict of interest

There is no conflict of interest.

Nomenclature

A	Area of droplet (mm^2)
Bo	Bond number
d_{eq}	Equivalent diameter of droplet(mm)
E	Aspect ratio
Eo	Eötvös number
g	Gravitational acceleration (m/s^2)
L	distance of falling (rising) of drop (m)
Mo	Morton number
Re	Reynolds number
t	Residence time(s)
V_t	Terminal Velocity(mm/s)
We	Weber number

Greek

μ_l	Viscosity of stagnant liquid (cp)
μ_d	Viscosity of droplet (cp)
ρ	Density ratio of droplet to continuous fluid
ρ_d	Density of droplet (kg/m^3)
ρ_l	Density of the stagnant liquid (kg/m^3)
σ	Surface tension between stagnant liquid and droplet (N/m)

References

Asokapandian, S., Sreelakshmi, S. & Rajamanickam, G., (2021). Lipids and Oils: An Overview. *Food biopolymers: Structural, functional and nutraceutical properties*, 389-411.

Azizi, Z., (2017). Experimental investigation of terminal velocity and Sherwood number of rising droplet in an extraction column. *Heat and Mass Transfer, 53*, 3027-3035.

Blanchette, F. & Bigioni, T. P., (2009). Dynamics of drop coalescence at fluid interfaces. *Journal of fluid mechanics, 620*, *333*.

Borzì, A. M., Biondi, A., Basile, F., Luca, S., Vicari, E. S. D. & Vacante, M., (2019). Olive oil effects on colorectal cancer. *Nutrients, 11*, *32*.

Brakstad, O. G., Nordtug, T. & Throne-Holst, M., (2015). Biodegradation of dispersed Macondo oil in seawater at low temperature and different oil droplet sizes. *Marine pollution bulletin, 93*, 144-152.

Charles, G. & Mason, S., (1960). The mechanism of partial coalescence of liquid drops at liquid/liquid interfaces. *Journal of Colloid Science, 15*, 105-122.

Clift, R., Grace, J. & Weber, M., (1978). *Bubbles, Drops and Particles*. *5*.

Cockbain, E. & McRoberts, T., (1953). The stability of elementary emulsion drops and emulsions. *Journal of Colloid Science, 8*, 440-451.

Deng, C., Huang, W., Wang, H., Cheng, S., He, X. & Xu, B., (2018). Preparation of micron-sized droplets and their hydrodynamic behavior in quiescent water. *Brazilian Journal of Chemical Engineering, 35*, 709-720.

Dong, T., Wang, F., Weheliye, W. H. & Angeli, P., (2020). Surfing of drops on moving liquid–liquid interfaces. *Journal of Fluid Mechanics, 892*.

Gopinath, A. & Koch, D. L., (2002). Collision and rebound of small droplets in an incompressible continuum gas. *Journal of Fluid Mechanics, 454*, 145- 201.

Gorzynik-Debicka, M., Przychodzen, P., Cappello, F., Kuban-Jankowska, A., Marino Gammazza, A., Knap, N., Wozniak, M. & Gorska-Ponikowska, M., (2018). Potential health benefits of olive oil and plant polyphenols. *International journal of molecular sciences, 19*, 686.

Grace, J., (1973). Shapes and velocities of bubbles rising in infinite liquid. *Transactions of the Institution of Chemical Engineers, 51*, 116-120.

Grace, J. R. (1976). Shapes and velocities of single drops and bubbles moving freely through immiscible liquids. *Transactions of the Institution of Chemical Engineers (English), 54*, 167-174.

Hartland, S. (1988). *Coalescence in Dense Packed Dispersion*, Ivanov, IB, Ed., in "Thin Liquid Films". Marcel Dekker, New York.

Hennenberg, M., Bisch, P. M., Vignes-Adler, M. & Sanfeld, A., (1979). Mass transfer, Marangoni effect, and instability of interfacial longitudinal waves: I. Diffusional exchanges. *Journal of Colloid and Interface Science, 69*, 128-137.

Hennenberg, M., Bisch, P. M., Vignes-Adler, M. & Sanfeld, A., (1980). Mass transfer, marangoni effect, and instability of interfacial longitudinal waves. II. Diffusional exchanges and adsorption—desorption processes. *Journal of Colloid and Interface Science, 74*, 495-508.

Jeffreys, G. V., & Davies, G. A. (1971). Coalescence of liquid droplets and liquid dispersion. In *Recent Advances in Liquid–Liquid Extraction* (pp. 495-584). Pergamon.

Karimi, S., Abiri, A., Shafiee, M. & Mohamadzadeh, N., (2020). Experimental Study on a Rising Oil Droplet through a Water-Oil Interface. *Journal of Mechanical Engineering, 51*, 361-368.

Karimi, S., Shafiee, M., Abiri, A. & Ghadam, F., (2019). The drag coefficient prediction of a rising bubble through a non-Newtonian fluid. *Amirkabir Journal of Mechanical Engineering, 52*, 71-80.

Karimi, S., Shafiee, M., Ghadam, F., Abiri, A. & Abbasi, H., (2020). Experimental study on drag coefficient of a rising bubble in the presence of rhamnolipid as a biosurfactant. *Journal of Dispersion Science and Technology, 42*, 835-845.

Khadiv, P. P. & Mousavian, S. M. A., (2004). Suggestion of new correlations for drop/interface coalescent phenomena in the and absence and presence of single surfactant. Iranian Journal of Chemistry and Chemical Engineering. *23*, 79-88.

Komrakova, A. E., (2019). Single drop breakup in turbulent flow. *The Canadian Journal of Chemical Engineering, 97*, 2727-2739.

Kurimoto, R., Hayashi, K. & Tomiyama, A., (2013). Terminal velocities of clean and fully-contaminated drops in vertical pipes. *International journal of multiphase flow, 49*, 8-23.

Laddha, G. & Degaleesan, T., (1983). Dispersion and coalescence. *TC Lo, MHI Baird, C. Hanson, ed*.

Linton, M. & Sutherland, K., (1956). The coalescence of liquid drops. *Journal of Colloid Science, 11*, 391-397.

Mao, N., Kang, C., Teng, S. & Mulbah, C., (2020). Formation and detachment of the enclosing water film as a bubble passes through the water-oil interface. *Colloids and Surfaces A: Physicochemical and Engineering Aspects, 586*, 124236.

Marcus, J. B. (2013). *Culinary nutrition: the science and practice of healthy cooking*. Academic Press.

Mohamed-Kassim, Z. & Longmire, E. K., (2003). Drop impact on a liquid–liquid interface. *Physics of Fluids, 15*, 3263-3273.

Mottola, M., Caruso, B. & Perillo, M. A., (2019). Langmuir films at the oil/water interface revisited. *Scientific reports, 9*, 1-13.

Nakache, E., Dupeyrat, M. & Vignes-Adler, M., (1983). Experimental and theoretical study of an interfacial instability at some oil—Water interfaces involving a surface-active agent: I. Physicochemical description and outlines for a theoretical approach. *Journal of Colloid and Interface Science, 94*, 187-200.

Psaltopoulou, T., Kosti, R. I., Haidopoulos, D., Dimopoulos, M. & Panagiotakos, D. B., (2011). Olive oil intake is inversely related to cancer prevalence: a systematic review and a meta-analysis of 13800 patients and 23340 controls in 19 observational studies. *Lipids in health and disease, 10*, 1-16.

Rao, A., Reddy, R. K., Ehrenhauser, F., Nandakumar, K., Thibodeaux, L. J., Rao, D. & Valsaraj, K. T., (2014). Effect of surfactant on the dynamics of a crude oil droplet in water column: Experimental and numerical investigation. *The Canadian Journal of Chemical Engineering, 92*, 2098-2114.

Reynolds, O., (1881). *On the floating of drops on the surface of water depending only on the purity of the surface*. Proc. Lit. Phil. Soc. Manchester, *21*.

Sinegribova, O. A., Andreev, A. Y., Voronin, O. V., Dvoeglazov, K. N., & Logsdail, D. (1993). The Influence of Silicic Acid on the Coalescence of Drop in the Extraction System TBP-HNO3 (HCl). *in Solvent Extraction in the Process Industries*, *3*.

Singh, K. & Bart, H.-J., (2020). Passage of a bubble through the interface between a shear-thinning heavier liquid and a Newtonian lighter liquid. *Chemical Engineering Communications, 207*, 790-807.

Singh, K., Gebauer, F. & Bart, H. J., (2017). Bouncing of a bubble at a liquid–liquid interface. *AIChE Journal, 63*, 3150-3157.

Slavtchev, S., Hennenberg, M., Legros, J.-C. & Lebon, G., (1998). Stationary solutal Marangoni instability in a two-layer system. *Journal of colloid and interface science, 203*, 354-368.

Slavtchev, S., Kalitzova-Kurteva, P. & Mendes, M., (2006). Marangoni instability of liquid–liquid systems with a surface-active solute. *Colloids and Surfaces A: Physicochemical and Engineering Aspects, 282*, 37-49.

Slavtchev, S. & Mendes, M., (2004). Marangoni instability in binary liquid–liquid systems. *International journal of heat and mass transfer, 47*, 3269-3278.

Stark, A. H., & Madar, Z. (2021). Olive oil in the prevention of breast and colon carcinogenesis. In *Olives and Olive Oil in Health and Disease Prevention* (pp. 337-345). Academic Press.

Sternling, C. a. & Scriven, L., (1959). Interfacial turbulence: hydrodynamic instability and the Marangoni effect. *AIChE Journal, 5*, 514-523.

Wang, S., Zhang, Y., Meredith, J. C., Behrens, S. H., Tripathi, M. K. & Sahu, K. C., (2018). The dynamics of rising oil-coated bubbles: experiments and simulations. *Soft matter, 14*, 2724-2734.

Wierzba, A., (1990). Deformation and breakup of liquid drops in a gas stream at nearly critical Weber numbers. *Experiments in fluids, 9*, 59-64.

Zawala, J., Krasowska, M., Dabros, T. & Malysa, K., (2007). Influence of bubble kinetic energy on its bouncing during collisions with various interfaces. *The Canadian Journal of Chemical Engineering, 85*, 669-678.

Zhang, C., Zhou, D., Sa, R. & Wu, Q., (2018). Investigation of single bubble rising velocity in LBE by transparent liquids similarity experiments. *Progress in Nuclear Energy, 108*, 204-213.

Zheng, K., Li, C., Yan, X., Zhang, H. & Wang, L., (2020). Prediction of bubble terminal velocity in surfactant aqueous solutions. *The Canadian Journal of Chemical Engineering, 98*, 607-615.